Journal of Information System and Technology Management
JISTM
EISSN: 0128-1666
Volume 11 Issue 44 (September 2026) PP. 236-257

JOURNAL OF INFORMATION SYSTEM AND TECHNOLOGY MANAGEMENT (JISTM)
www.gaexcellence.com/jistm

POINT CLOUD PROCESSING ON 3D LIDAR DATA FOR UNMANNED SURFACE VEHICLES NAVIGATION IN MARINE ENVIRONMENTS

Aiman Norazaruddin[1]*, Zulkifli Zainal Abidin[2]

[1]Department of Mechatronics Engineering, Kulliyyah of Engineering, International Islamic University Malaysia, Malaysia
aiman.norazaruddin@gmail.com https://orcid.org/0009-0002-3651-3396
2Department of Mechatronics Engineering, Kulliyyah of Engineering, International Islamic University Malaysia, Malaysia
zzulkifli@iium.edu.my https://orcid.org/0000-0003-3559-2440
*Corresponding Author

Article Info:

Article history:
Received date: 28.06.2026
Revised date: 12.07.2026
Accepted date: 04.08.2026
Published date: 15.09.2026

To cite this document:

Norazaruddin, A., & Abidin, Z. Z. (2026). Point Cloud Processing On 3D Lidar Data for Unmanned Surface Vehicles Navigation in Marine Environments. *Journal of Information System and Technology Management, 11* (44), 236-257.

Abstract:

Unmanned Surface Vehicles (USVs) require reliable autonomous navigation systems in dynamic maritime environments. LiDAR sensors, while effective for obstacle detection, are susceptible to noise and distortion from wave oscillations and water surface absorption, generating false positives and negatives in point cloud data. Most existing preprocessing-clustering evaluations are confined to terrestrial or simulated settings, with limited benchmarking under real maritime conditions marked by wave-induced motion, surface reflections, and sparse returns. This study addresses that gap through one of the first systematic evaluations of preprocessing-clustering combinations using real harbour LiDAR data collected under genuine environmental disturbance. A Velodyne HDL-32E LiDAR sensor was deployed at Klang Harbour, Malaysia, to collect real-world point cloud datasets. Three preprocessing techniques — Voxel Grid Downsampling, Statistical Outlier Removal (SOR), and Radius Outlier Removal (ROR) — were evaluated with two clustering algorithms chosen for their contrasting noise-handling strategies: Density-Based Spatial Clustering of Applications with Noise (DBSCAN) and Euclidean Cluster Extraction (ECE). Performance was assessed using precision and accuracy against manually annotated ground truth. DBSCAN combined with SOR achieved the highest performance, with peak accuracy of 57% ($\varepsilon = 1.0$ m) and peak precision of 62% ($\varepsilon = 2.0$ m), as SOR removes wave-induced outliers while preserving obstacle geometry, enabling DBSCAN's density criterion to isolate genuine clusters more reliably. ROR consistently degraded performance by over-removing genuine sparse returns, while ECE underperformed across all configurations due to its lack of native noise handling. The overall pipeline reached approximately 60% accuracy, a modest ceiling reflecting persistent wave motion, surface reflections, sparse long-range returns, and moving vessels that geometry-based clustering alone cannot resolve. This study contributes a methodological benchmark for preprocessing-clustering pipeline selection in maritime LiDAR processing, and practical guidance for selecting efficient, noise-robust configurations for real-time USV obstacle detection. Future work should incorporate model-based object detection and multi-sensor fusion to improve classification capability and system reliability.

DOI: 10.35631/JISTM.1144015

Keyword:

Clustering, DBSCAN, LiDAR, Maritime Navigation, Point Cloud Processing, Statistical Outlier Removal, Unmanned Surface Vehicle

Introduction

The increasing deployment of autonomous systems in maritime operations has accelerated demand for reliable Unmanned Surface Vehicles (USVs) capable of navigating complex, dynamic environments without human intervention as shown in Figure 1. USVs have demonstrated significant potential across oceanographic research, environmental monitoring, port logistics, and defence applications, owing to their capacity to operate continuously in hazardous conditions while substantially reducing human risk and operational costs (Liu et al., 2016; Manley, 2008).

Figure 1: Sensors Deployed for Unmanned Surface Vessel (USV) Autonomous Navigation

Journal of Information System and Technology Management
JISTM
EISSN: 0128-1666
Volume 11 Issue 44 (September 2026) PP. 236-257
The Guidance, Navigation, and Control (GNC) systems of Unmanned Surface Vessels (USVs) rely heavily on exteroceptive sensors, with 3D LiDAR emerging as a crucial modality for generating high-resolution, range-accurate spatial data. However, deploying LiDAR in nearshore maritime environments introduces severe perception challenges. Infrared beam absorption by water surfaces leads to sparse point clouds, while wave-induced oscillations generate systematic noise, resulting in false readings that compromise obstacle detection integrity (Zhou et al., 2021). Furthermore, the substantial computational burden of large-scale point cloud datasets necessitates efficient processing to enable real-time autonomous navigation amidst dynamic reflections and frequent occlusions (Balta et al., 2018; Bovcon et al., 2021).

To mitigate these environmental artifacts, sequential processing pipelines utilizing filtering techniques—such as Voxel Grid Downsampling, Statistical Outlier Removal (SOR), and Radius Outlier Removal (ROR)—are essential before applying clustering algorithms like DBSCAN or Euclidean Cluster Extraction (ECE) for obstacle segmentation. Despite the theoretical efficacy of these methods, their comparative performance and the compound effects of specific preprocessing-clustering combinations remain insufficiently benchmarked under real-world maritime conditions. The optimal configuration required to sustain reliable perception in dynamic, high-density nearshore scenarios is currently undefined in the literature. Addressing this critical gap, this study systematically evaluates various preprocessing and clustering configurations using empirical 3D LiDAR data collected at Klang Harbour, Malaysia. The primary objectives are to quantify the impact of Voxel Grid, SOR, and ROR techniques on point cloud quality; compare the accuracy and precision of DBSCAN versus ECE under varying parameters; and ultimately establish an optimized perception pipeline for USV obstacle detection. This research contributes to a broader initiative at the Centre for Unmanned Technologies (CUTe), International Islamic University Malaysia, to develop resilient autonomous navigation frameworks for nearshore operations.

The novelty of this work lies in its evaluation of preprocessing-clustering combinations using empirical, harbour-collected LiDAR data under genuine environmental disturbance rather than simulated or terrestrial benchmarks; to the authors' knowledge, this constitutes one of the first systematic comparative evaluations of its kind for maritime obstacle detection. This study makes two principal contributions. Methodologically, it provides a comparative performance benchmark of preprocessing and clustering pipelines applicable to real-world maritime LiDAR processing, characterising the compound effects of specific preprocessing-clustering combinations that prior terrestrial- or simulation-based studies do not capture. Practically, it offers guidance for selecting computationally efficient, noise-robust preprocessing-clustering configurations suited to onboard USV deployment in nearshore environments.

Literature Review

Unmanned Surface Vehicles

USVs are autonomous maritime vessels capable of operating without an onboard human crew, independently or under semi-autonomous supervision. Liu et al. (2016) provide a comprehensive overview of USV developments and challenges, noting that USVs face inherent difficulties in achieving reliable GNC operations, particularly in complex or hazardous environments. Key advantages of USVs over manned vessels include extended operational endurance, immunity to crew fatigue, reduced maintenance costs, and compact structural

Journal of Information System and Technology Management
JISTM
EISSN: 0128-1666
Volume 11 Issue 44 (September 2026) PP. 236-257
designs enabling deployment in shallow waters. Applications span environmental monitoring, oceanographic surveying, port security, maritime logistics, and military operations (Manley, 2008; Ahmed et al., 2023).

The structural architecture of a USV consists of six fundamental elements: the hull and auxiliary structure, propulsion and power systems, the GNC system, communication systems, data collection equipment, and a ground station. The GNC system — comprising guidance, navigation, and control subsystems — is the most critical element, as illustrated in Figure 2. The navigation subsystem is responsible for interpreting environmental sensor data and transmitting actionable information to the guidance and control layers, which govern trajectory planning and actuator commands respectively (Liu et al., 2016).

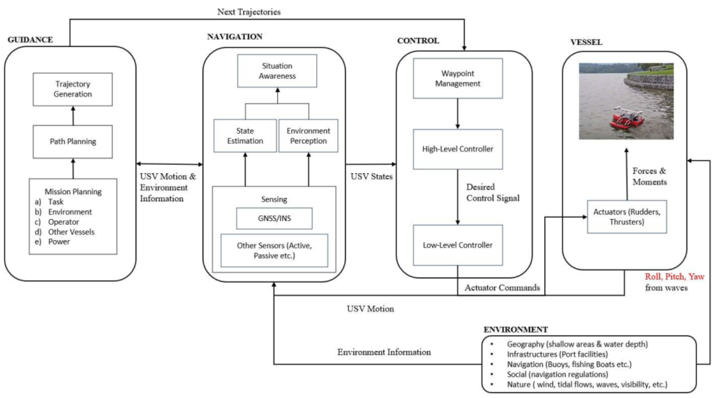

Figure 2: GNC Subsystem Relationship Illustrating the Interconnection Between Navigation, Guidance, and Control Layers in a USV.

The demand for USV technology is further driven by advancements in GPS compactness and affordability, improved wireless communication bandwidth, and the increasing capability of artificial intelligence platforms for onboard computation (Manley, 2008). Several software architectures support USV perception and navigation tasks, including the MOOS-IvP framework for mission-oriented autonomous operation and ROS-based implementations adapted from terrestrial robotics (Benjamin et al., 2010). Contemporary USV systems increasingly implement multimodal sensor fusion frameworks combining LiDAR, cameras, radar, sonar, GPS/GNSS, and inertial navigation systems to generate a comprehensive situational picture (Feng et al., 2020).

LiDAR in Maritime Environments

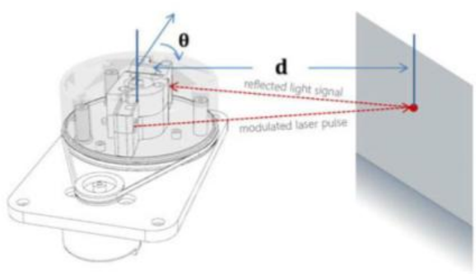

Figure 3: LiDAR System Mechanism Working in 2D Space.

Journal of Information System and Technology Management
JISTM
EISSN: 0128-1666
Volume 11 Issue 44 (September 2026) PP. 236-257
LiDAR (Light Detection and Ranging) is an active sensor that measures spatial, spectral, and temporal data to determine the distance to objects through Time-of-Flight (ToF) measurement as illustrated in Figure 3. The fundamental operating principle relies on calculating the elapsed time between the emission of an infrared pulse and the detection of its reflection, as expressed in equation (1), where d is the measured distance, C is the speed of light, and Δt is the round-trip time (Jin et al., 2019).

$$d = \frac{C \times \Delta t}{2} \quad (1)$$

LiDAR architectures are classified by dimensionality into 1D (single-axis distance), 2D (horizontal plane scanning), and 3D (combined horizontal and vertical plane) systems. A 3D LiDAR system comprises four primary subsystems: the beam deflection unit, range finding unit, power supply unit, and controller unit. The horizontal and vertical fields of view (FOV) of a 3D LiDAR are governed by azimuth and elevation angles, with horizontal and vertical resolutions defined by equations (2) – (5).

$$FOV_{\mathrm{h}} = \theta_2 - \theta_1 \quad (2)$$

$$FOV_{\mathrm{v}} = \varphi_2 - \varphi_1 \quad (3)$$

$$H_{res} = \frac{FOV_{\mathrm{h}}}{d\theta} \quad (4)$$

$$V_{res} = \frac{FOV_{\mathrm{v}}}{d\varphi} \quad (5)$$

Whilst LiDAR provides high-precision range data in terrestrial and urban applications, its deployment in maritime environments introduces significant limitations. Zhou et al. (2021) demonstrate that water surfaces absorb rather than reflect infrared beams, producing sparse point cloud density with substantially fewer data points than equivalent land-based scans. Furthermore, wave-induced oscillations impose systematic distortions: the random motion of a USV-mounted LiDAR alters the geometric correspondence between successive scans, generating outlier points and reducing the effectiveness of point matching algorithms. These characteristics necessitate robust preprocessing before any mapping or clustering operation can yield reliable obstacle representations.

LiDAR selection for USV applications requires consideration of four specification categories in order of priority: range (maximum and minimum detection distance, resolution, update frequency), physical (size, weight, power consumption), laser (wavelength, class, power), and optical (beam divergence, focal length) properties. For nearshore maritime navigation, long-range capability, high point density, and mechanical robustness against vibration and moisture are primary selection criteria (Rhinal et al., 2020).

Environmental Challenges in Nearshore Navigation

Nearshore maritime environments present a complex operational domain for USV perception systems. Unlike open-water scenarios where navigational hazards are relatively sparse, nearshore zones exhibit dense static and dynamic obstacles including piers, jetties, floating debris, recreational vessels, and wildlife. Four principal environmental challenges affect LiDAR-based perception in this context.

First, water surface reflections introduce phantom point artefacts: specular reflections cause LiDAR beams to reflect off calm or partially reflective water surfaces, creating spurious

Journal of Information System and Technology Management
JISTM
EISSN: 0128-1666
Volume 11 Issue 44 (September 2026) PP. 236-257

coordinates that cannot be distinguished from real obstacles without preprocessing. Under high-glare conditions, interference with both optical and laser-based sensing is substantially elevated (Damodaran et al., 2023). Second, wave interference imposes continuous vertical displacement and pitch/roll motion on the USV platform, degrading the spatial alignment between successive LiDAR scans and introducing noise into the resultant point cloud. This wave-induced motion is particularly challenging for multi-sensor calibration, as extrinsic parameters between LiDAR and co-mounted sensors may drift under sustained mechanical stress (Bovcon et al., 2021).

Third, occlusion is pronounced in congested waterways: objects partially hidden behind structures or vessels may be entirely absent from LiDAR sweeps at the USV's low sensor vantage point, creating gaps in the obstacle representation. Fourth, variable lighting conditions — ranging from intense daytime glare to low-light dawn and dusk scenarios — affect camera-based sensors co-deployed with LiDAR. Although LiDAR itself is largely illumination-independent, its fusion with visual sensors requires robust handling of lighting variation. Additionally, biological clutter from floating vegetation, marine animals, and wave foam can trigger false detections if perception algorithms are not trained on sufficiently diverse maritime datasets (Talpur et al., 2025).

Point Cloud Preprocessing

Downsampling Algorithm

Given the noise characteristics of maritime LiDAR data, preprocessing is a critical pipeline stage before obstacle clustering. Three principal techniques are employed in this study: Voxel Grid Downsampling, Statistical Outlier Removal (SOR), and Radius Outlier Removal (ROR). These were selected because they are the most widely adopted, computationally lightweight preprocessing methods in the point cloud literature and, in combination, target distinct and complementary noise mechanisms — spatial density normalisation, statistically-informed outlier removal, and density-threshold-based outlier removal, respectively — allowing their individual and combined contributions to downstream clustering performance to be isolated. Figure 4 illustrates the general preprocessing block diagram, showing the data flow from raw point cloud input through subsampling and filtering to the refined output used for 3D modelling and clustering.

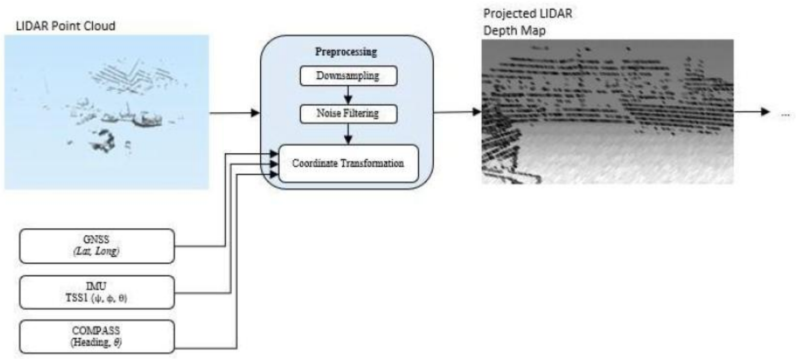

Figure 4: Block Diagram of the Point Cloud Preprocessing Pipeline

Voxel Grid Downsampling partitions the three-dimensional point cloud space into uniform cubic volumes, known as voxels, each of side length V. For each occupied voxel, a single centroid representative point is computed as the arithmetic mean of all contained coordinates. The number of voxels along each spatial dimension is calculated in equations (6) – (9) (Hacinecipoglu, 2022).

$$M_x = \frac{X_{\max} - X_{\min}}{V} \tag{6}$$

$$M_y = \frac{Y_{\max} - Y_{\min}}{V} \tag{7}$$

$$M_z = \frac{Z_{\max} - Z_{\min}}{V} \tag{8}$$

$$M_{total} = M_x \times M_y \times M_z \tag{9}$$

The centroid coordinates (C_x, C_y, C_z) for each voxel containing N points are computed in equations (10).

$$C_x = \frac{1}{N}\sum_{i=1}^{N} x_i \,, C_y = \frac{1}{N}\sum_{i=1}^{N} y_i \,, C_z = \frac{1}{N}\sum_{i=1}^{N} z_i \tag{10}$$

This approach reduces the dataset to M_total representative points without significant loss of structural features, while promoting near-uniform spatial density across the sensor's measurement volume (Balta et al., 2018). The pseudocode developed for the voxel grid downsampling preprocessing is shown in the algorithm below:

input: P = Point Cloud Data; voxSize = Voxel size
output: V, voxelGrid
for point **in** pointCloud: //iterate for each point
    voxelIndexX = round(point.x / voxelSize); voxelIndexY = round(point.y / voxelSize);
    voxelIndexZ = round(point.z / voxelSize)
    if (voxelIndexX, voxelIndexY, voxelIndexZ) in voxelGrid:
        add point.x to arrayX; point.z to arrayY; point.z to arrayZ
        find centre point $C_x = \frac{1}{N}\sum_{i=1}^{N} x_i \,, C_y = \frac{1}{N}\sum_{i=1}^{N} y_i \,, C_z = \frac{1}{N}\sum_{i=1}^{N} z_i$
        voxelGrid[(voxelIndexX, voxelIndexY, voxelIndexZ)] = centre point
    else:
        voxelGrid[(voxelIndexX, voxelIndexY, voxelIndexZ)] = point

Noise Reduction Algorithm

Statistical Outlier Removal (SOR) identifies and eliminates points whose neighbourhood distance distributions deviate beyond a statistically defined threshold. For each point p_i, the mean distance μ and standard deviation σ of distances to all neighbouring points within a radius r are computed in equations (11) – (13).

$$\mu = \frac{1}{N}\sum_{i=1}^{N} d_i \tag{11}$$

$$\sigma = \sqrt{\frac{1}{N}\sum_{i=1}^{N} (d_i - \mu)^2} \tag{12}$$

Journal of Information System and Technology Management
JISTM
EISSN: 0128-1666
Volume 11 Issue 44 (September 2026) PP. 236-257

$$range = \mu \pm k\sigma \tag{13}$$

$$\text{Outlier criterion: } d_{\text{mean}} \in [\mu - k\sigma,\ \mu + k\sigma] \tag{14}$$

A point is classified as an outlier and discarded if its mean neighbourhood distance falls outside the range of the criterion, where k is the standard deviation multiplier that governs the filter's aggressiveness as described in equation (14). The algorithm for the noise removal process is described below:

input: P = Point Cloud Data; k = standard deviation multiplier, r = radius
output: F, filtered points
for point in pointCloud: //iterate for each point
    if point not in visitedPointCloud array:
        append to visitedPointCloud array
    for neighbourPt **in** pointCloud: find euclidean distance, d, for every other point
        if d < r: **append** to neighbour array
    calculate μ, mean and σ, standard deviation
    calculate range = $\mu \pm k\sigma$
    if point between range
        append to f, filtered point cluster
    else:
        continue

A computationally efficient variant, Fast Cluster Statistical Outlier Removal (FCSOR), employs dimensionality reduction and cluster-based processing to achieve equivalent noise removal with reduced memory and processing time, making it more suitable for real-time USV applications (Balta et al., 2018). Figure 5 illustrates the qualitative effect of SOR preprocessing on a maritime point cloud dataset, demonstrating the reduction of noise artefacts while preserving obstacle geometry.

(a) (b)

Figure 5: (a) Raw Maritime Point Cloud (b) Preprocessed Version After SOR.

Radius Outlier Removal (ROR) provides an alternative noise removal strategy based on spatial point density rather than statistical distribution. For each point p_i, the algorithm counts N_r neighbours within a defined radius r. Points failing to satisfy the minimum neighbour count condition (N_r < N_min) are classified as outliers and removed.

Unlike SOR, ROR does not apply statistical range analysis, making it computationally simpler but inherently less discriminative in environments where genuine low-density regions coexist alongside noise artefacts — a condition particularly common in maritime point clouds due to water surface absorption (Szutor & Zichar, 2023). The high computational cost of Nearest

Journal of Information System and Technology Management
JISTM
EISSN: 0128-1666
Volume 11 Issue 44 (September 2026) PP. 236-257
Neighbour (NN) search used in both SOR and ROR represents a practical constraint for real-time onboard processing.

Clustering Algorithms for Point Cloud Segmentation

Following preprocessing, clustering algorithms segment the refined point cloud into discrete object representations. These representations are subsequently used to estimate obstacle position and extent for navigation decisions. DBSCAN and ECE were selected for evaluation because they represent the two dominant paradigms in unsupervised point cloud clustering — density-based and distance-based grouping, respectively — and, unlike model-based object detectors that require extensive labelled training data, both are computationally tractable for real-time onboard deployment, making them directly comparable candidates for a maritime obstacle-detection pipeline.

DBSCAN (Density-Based Spatial Clustering of Applications with Noise) clusters points by spatial density, grouping all points within an epsilon radius (ε) that satisfy a minimum point count (minPts). Points failing this criterion are assigned as noise and excluded from any cluster. Cluster expansion continues iteratively until all density-reachable points within the neighbourhood are assigned.

$$|N_\varepsilon(p)| \geq minPts \tag{15}$$

The core condition for a point p to be considered a core point is described in equation (15) where $N_\varepsilon(p)$ denotes the set of points within distance ε of p. DBSCAN's inherent noise-resistance makes it well-suited to environments with irregular point distributions (Yu Cao et al., 2021), though its computational complexity depending on spatial indexing strategy demands substantial memory for large-scale maritime datasets.

Euclidean Cluster Extraction (ECE) groups points based on a maximum Euclidean distance threshold (maxDistance) between neighbouring points. Two points p_i and p_j are assigned to the same cluster if their Euclidean distance satisfies the proximity condition as described in equation (16).

$$d(p_i, p_j) = \sqrt{(x_i - x_j)^2 + (y_i - y_j)^2 + (z_i - z_j)^2} \leq \text{maxDistance} \tag{16}$$

ECE lacks native noise handling and does not adaptively manage cluster sizing, which may limit performance in the irregular density conditions characteristic of maritime LiDAR scans. Li et al. (2019) applied ECE to urban point cloud road inventory with effective structural differentiation; however, the fixed-size cluster constraints and absence of noise labelling represent a significant limitation for dynamic maritime obstacle scenarios.

Performance Metrics

Clustering performance is evaluated by comparing detected clusters against manually annotated ground truth bounding boxes. Four classification outcomes form the basis of performance calculation: True Positives (TP) — clustered points correctly falling within ground truth regions; False Positives (FP) — clustered points outside ground truth boundaries; False Negatives (FN) — unclustered points within ground truth regions; and True Negatives

Journal of Information System and Technology Management
JISTM
EISSN: 0128-1666
Volume 11 Issue 44 (September 2026) PP. 236-257
(TN) — unclustered points correctly outside ground truth boundaries. Precision and accuracy are defined in equations (17) and (18).

$$\text{Precision} = \frac{TP}{TP + FP} \tag{17}$$

$$\text{Accuracy} = \frac{TP + TN}{TP + FP + TN + FN} \tag{18}$$

These metrics provide complementary assessments: precision measures the correctness of positive predictions (minimising false obstacle detections), while accuracy evaluates overall classification correctness across all point assignments. Average Precision (AP), defined as the area under the precision-recall curve at varying IoU thresholds, is additionally used in 3D object detection literature to provide a unified detection quality measure (Yu Cao et al., 2021).

Research Gaps and Study Rationale

A review of existing literature reveals several persistent gaps. First, whilst LiDAR preprocessing and clustering methods have been extensively studied for terrestrial applications (autonomous driving, urban mapping), their systematic comparative evaluation under real maritime conditions is limited. Most studies either use simulated data or report results without controlled parameter variation. Second, the combined effect of preprocessing algorithm choice on downstream clustering performance — specifically whether SOR or ROR better prepares point clouds for DBSCAN versus ECE — has not been empirically characterised in maritime environments. Third, the optimal parameter ranges (epsilon for DBSCAN, maxDistance for ECE, radius and k for SOR/ROR) for harbour-scale obstacle scenes remain undetermined from field data. This study directly addresses these gaps through systematic experimentation at a real maritime site under representative harbour conditions.

Methodology

Experimental Setup and Data Collection

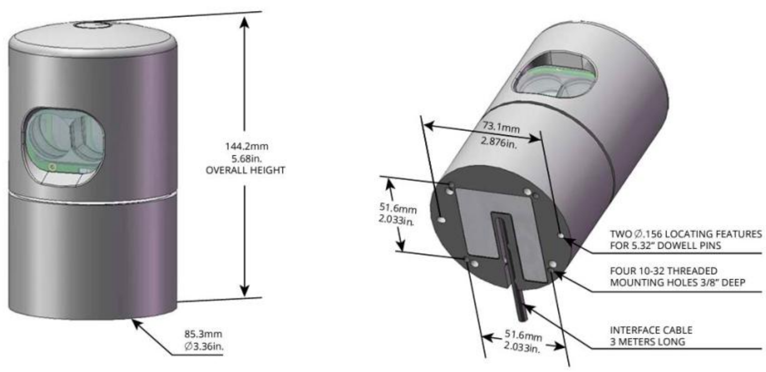

Figure 6: Velodyne HDL-32E LiDAR Sensor

Point cloud data were collected at Klang Harbour, Malaysia, aboard a remote-controlled surface vessel equipped with a Velodyne HDL-32E 3D LiDAR sensor (Figure 6). The HDL-32E is a high-performance 32-channel rotating LiDAR capable of generating approximately

Journal of Information System and Technology Management
JISTM
EISSN: 0128-1666
Volume 11 Issue 44 (September 2026) PP. 236-257
695,000 points per second in single return mode (approximately 1,390,000 in double return mode), with a 100 m detection range and ±2 cm range accuracy. Full sensor specifications are presented in Table 1. The sensor was mounted at the vessel bow and connected to a ROS (Robot Operating System) node for real-time data recording and streaming. Figure 7 presents the overall research methodology flowchart, illustrating the iterative pipeline from data collection through preprocessing, clustering, and validation.

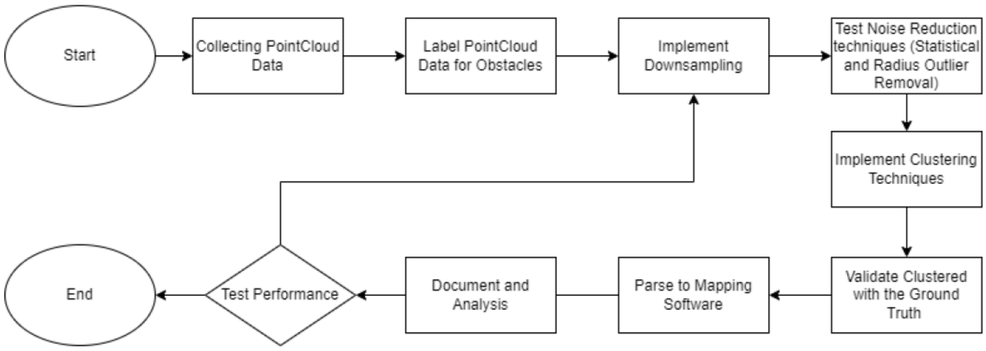

Figure 7: Proposed Research Methodology Flowchart.

Table 1: Velodyne HDL-32E LiDAR Specifications

Category	Parameter	Value
Range	Detection Range	100 m
Range	Range Accuracy	±2 cm
Field of View	Vertical FOV	41.33°
Field of View	Horizontal FOV	360°
Resolution	Angular Res. (Vertical)	1.33°
Resolution	Angular Res. (Horizontal)	0.08°
Output	Points/sec (Single Return)	~695,000
Output	Points/sec (Double Return)	~1,390,000
Electrical	Power Consumption	12 W
Electrical	Operating Voltage	9 V – 18 V

Data were recorded across two maritime scenarios representative of typical harbour conditions: a pier launch environment (Figure 8a) and a bay containing sea structures and floating obstacles (Figure 8b). The pier environment features multiple bridge supports and a quayside wall at close range, providing dense, high confidence point returns with minimal wave interference. The bay environment introduces greater environmental variability including open water surfaces, floating buoys, moored vessels, and wave-induced motion, testing the robustness of preprocessing under more challenging conditions. Multiple point cloud frames were collected in each environment to provide a statistically representative evaluation dataset.

Journal of Information System and Technology Management
JISTM
EISSN: 0128-1666
Volume 11 Issue 44 (September 2026) PP. 236-257

(a) **(b)**

Figure 8: Maritime Data Collection Environments: (a) Pier Launch Site; (b) Bay Area with Sea Structures and Floating Obstacles.

Point Cloud Annotation and Ground Truth Establishment

Manual annotation of collected point cloud data was performed using LabelCloud software to establish ground truth bounding boxes for all obstacle clusters, as shown in Figure 9. LabelCloud provides a graphical user interface for placing and sizing 3D bounding boxes aligned with obstacle boundaries in the point cloud space. Each annotated label includes the box centroid coordinates, dimensions (width, height, length), rotation angle, and an obstacle class label (e.g., vessel, buoy, coastline structure). Annotated labels were exported in both .bin and .pcd file formats for compatibility with the evaluation pipeline. A total of five obstacle categories were labelled: pier structures, vessel hulls, buoys, coastline walls, and miscellaneous debris.

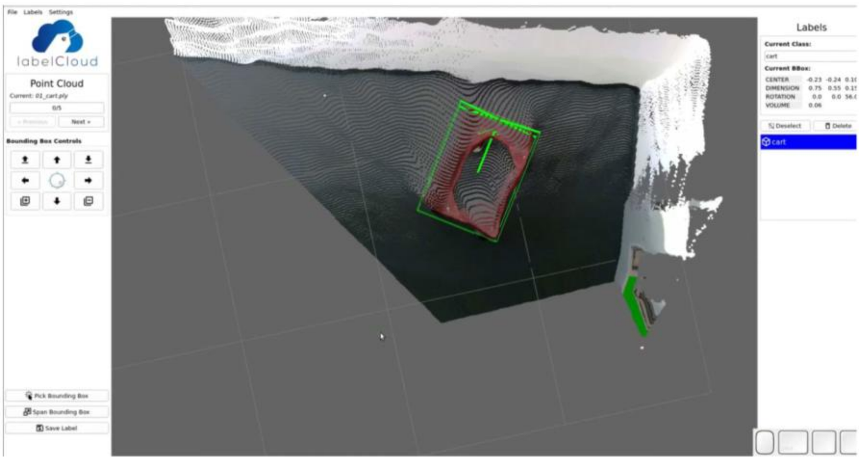

Figure 9: Ground Truth Annotation Interface in LabelCloud Software Showing 3D Bounding Boxes Applied to Maritime Point Cloud Data.

Preprocessing Pipeline

Three preprocessing techniques were applied and evaluated independently prior to clustering. The preprocessing pipeline processes raw LiDAR point clouds in three stages: downsampling for density normalisation, statistical or radius-based noise removal for outlier elimination, and the resulting filtered point cloud is passed to the clustering stage.

Journal of Information System and Technology Management
JISTM
EISSN: 0128-1666
Volume 11 Issue 44 (September 2026) PP. 236-257
Voxel Grid Downsampling was applied with voxel sizes V of 0.05, 0.10, 0.20, and 0.30 m. For each point p = (x, y, z) in the input cloud, the voxel index is computed, and a single centroid representative is retained per occupied voxel. The effect of voxel size on computational reduction is characterised by the average point count drop metric defined in Equation (19).

$$\text{Avg Pt Drop} = \frac{1}{N}\sum_{i=1}^{N}(\text{Original Points}_i - \text{Downsampled Points}_i) \tag{19}$$

SOR noise removal was applied to the downsampled cloud with the standard deviation multiplier k varied across {0.5, 1.0, 1.5, 2.0} and the neighbourhood radius r varied across {0.5, 1.0, 1.5, 2.0} m. For each query point, the algorithm identifies all neighbours within radius r, computes their mean distance μ and standard deviation σ, and discards the point if its mean neighbourhood distance lies outside. Each combination of k and r was evaluated independently to isolate their individual effects on point reduction rate.

ROR noise removal was evaluated by varying the search radius r across {1.0, 1.5, 2.0, 2.5} m at fixed minimum neighbour count N_min = 5, and by varying N_min across {2, 4, 6, 8} at fixed r = 1.0 m. This orthogonal parameter sweep decouples the contributions of search radius and density threshold to the overall point elimination rate.

Clustering Pipeline

Two clustering algorithms were evaluated on the preprocessed point clouds. All clustering trials used a baseline voxel downsampling of v = 0.10 m as the primary density normalisation step, with either SOR or ROR applied as the subsequent noise removal stage, or no further preprocessing as a control condition.

For DBSCAN, the epsilon radius ε was systematically varied across five levels: {0.5, 1.0, 2.0, 3.0, 4.0} m, with each level evaluated under three preprocessing conditions: no noise removal, SOR (k = 1.0, r = 1.0), and ROR (r = 1.0, N_min = 5). The DBSCAN algorithm iterates over all unvisited points, expanding clusters by adding all density-reachable neighbours recursively until no further expansion satisfies the core point condition. Points failing this condition are labelled as noise.

For ECE, the maximum Euclidean distance threshold (maxDistance) was varied across {1.0, 2.0, 3.0} m under the same three preprocessing conditions. ECE iteratively assigns each unvisited point to a cluster by finding all neighbours within maxDistance, then expanding recursively from those neighbours. No noise labelling is performed; all points are assigned to the cluster of the nearest already-clustered point or to a new cluster if no neighbour is within maxDistance.

Performance Evaluation

Clustering performance was quantified against the manually annotated ground truth bounding boxes using precision and accuracy. True Positives (TP) represent clustered points correctly falling within ground truth boundaries; False Positives (FP) are clustered points outside ground truth boundaries; False Negatives (FN) are unclustered points within ground truth regions; and True Negatives (TN) are unclustered points correctly outside ground truth boundaries. All

Journal of Information System and Technology Management
JISTM
EISSN: 0128-1666
Volume 11 Issue 44 (September 2026) PP. 236-257
metrics were computed at the point level rather than the cluster level, providing fine-grained assessment of spatial coverage.

For preprocessing evaluation, the average point cloud count drop served as the primary dependent variable, characterising how aggressively each parameter configuration removes points. This metric was computed as the mean across all collected dataset frames for each parameter setting, providing a scene-averaged estimate of point reduction rather than a single-frame measurement.

Results

Downsampling Performance

Table 2 presents the average point cloud count reduction as a function of voxel size. Results confirm a monotonic and approximately exponential relationship between voxel size and point elimination: increasing voxel size from 0.05 m to 0.30 m raised the average point count reduction from 1,379 to 13,703 points. The rate of increase is non-linear — moving from 0.05 to 0.10 m eliminates 3× more points than the initial step, and the jump from 0.20 to 0.30 m adds only 3,295 additional eliminated points despite the same 0.10 m increment, suggesting diminishing returns at coarser voxel sizes in the harbour dataset.

Table 2: Voxel Grid Downsampling Results

Iteration	Voxel Size (m)	Avg. Point Count Drop
1	0.05	1,379
2	0.10	4,183
3	0.20	10,408
4	0.30	13,703

This behaviour is consistent with the mathematical formulation: larger voxels encompass greater volumes (V^3 scaling), causing more raw points to be merged into single centroid representatives. At v = 0.30 m, the 13,703-point average reduction represents a substantial computational saving, though at the cost of potential loss of fine structural features for small obstacles such as buoys and mooring lines. Voxel size v = 0.10 m was selected as the clustering baseline, providing a meaningful density reduction (4,183 points average) whilst preserving obstacle-relevant spatial features at sub-obstacle resolution.

SOR Noise Removal Performance

Tables 3a and 3b present SOR results for varying k and r respectively. Two independent trends are observed. First, increasing the standard deviation multiplier k at fixed r = 1.0 m produces a non-monotonic effect: point elimination increases from k = 0.5 (8,461 points) through k = 1.0 (9,418 points) and peaks at k = 2.0 (12,681 points), with the anomalous result at k = 1.5 (9,328 points, slightly below k = 1.0) likely reflecting frame-to-frame variability in the collected dataset. As k increases, the acceptance window $[\mu - k\sigma, \mu + k\sigma]$ widens, which should retain more points; however, the radius r influences which points contribute to μ and σ, potentially causing complex interactions with point density distribution in the harbour scene.

Journal of Information System and Technology Management
JISTM
EISSN: 0128-1666
Volume 11 Issue 44 (September 2026) PP. 236-257

Table 3a: SOR Results — Varying Standard Deviation Multiplier k (r = 1.0 m)

Iteration	k (Std Dev Multiplier)	r (Radius, m)	Avg. Point Count Drop
1	0.5	1.0	8,461
2	1.0	1.0	9,418
3	1.5	1.0	9,328
4	2.0	1.0	12,681

Table 3b: SOR Results — Varying Radius r (k = 1.0)

Iteration	k (Std Dev Multiplier)	r (Radius, m)	Avg. Point Count Drop
5	1.0	0.5	6,322
6	1.0	1.5	13,404
7	1.0	2.0	13,822

The effect of radius r is more pronounced and consistent: doubling r from 0.5 to 1.0 m increases point elimination from 6,322 to 9,418 (+49%) and further increases to 1.5 m and 2.0 m produce 13,404 and 13,822 eliminations respectively. This monotonic increase reflects the expanded neighbourhood considered when computing μ and σ: larger radii incorporate more distant points, causing the mean and standard deviation to stabilise toward global estimates, which flag more locally sparse points as outliers. The near-plateau between r = 1.5 m and r = 2.0 m (only 418-point difference) suggests that at $r \geq 1.5$ m, the neighbourhood statistics approach the scene-level distribution, beyond which further radius increases yield diminishing elimination benefits.

ROR Noise Removal Performance

Table 4a: ROR Results — Varying Radius (N_min = 5)

Iteration	Radius (m)	Min. Points	Avg. Point Count Drop
1	1.0	5	7,744
2	1.5	5	8,512
3	2.0	5	9,724
4	2.5	5	14,234

Table 4b: ROR Results — Varying Minimum Point Count (r = 1.0 m)

Iteration	Radius (m)	Min. Points	Avg. Point Count Drop
5	1.0	2	8,967
6	1.0	4	8,302
7	1.0	6	3,782
8	1.0	8	1,639

ROR exhibits clearly monotonic trends in both parameter dimensions, providing more interpretable behaviour than SOR. Increasing the search radius r from 1.0 to 2.5 m at fixed N_min = 5 progressively increases point elimination from 7,744 to 14,234, as larger search

Journal of Information System and Technology Management
JISTM
EISSN: 0128-1666
Volume 11 Issue 44 (September 2026) PP. 236-257

spheres include more points in the density count, making it harder for sparse points to satisfy the minimum count threshold. Notably, the elimination jumps between r = 2.0 m (9,724) and r = 2.5 m (14,234) — a 46% increase — is substantially larger than previous steps, suggesting the r = 2.5 m radius crosses a critical density threshold in the harbour dataset where a significant proportion of points have fewer than 5 neighbours.

Increasing N_min at fixed r = 1.0 m produces the opposite effect: higher minimum count requirements reduce elimination from 8,967 (N_min = 2) to 1,639 (N_min = 8). This counterintuitive result — stricter density criteria removing fewer points — reflects the sparse character of maritime LiDAR data: with N_min = 8, most genuine low-density regions fail the threshold alongside noise points, effectively treating the entire point cloud as "below threshold" and removing everything except densely clustered returns. At N_min = 8, ROR may be inadvertently suppressing valid obstacle points in open water regions. The inflection between N_min = 4 and N_min = 6 (8,302 to 3,782 points) is particularly sharp, identifying N_min = 5 as a practical boundary.

DBSCAN Clustering Performance

Table 5 presents DBSCAN clustering accuracy and precision across all epsilon values and preprocessing conditions. The results reveal consistent patterns across the parameter space.

Table 5: DBSCAN Clustering Results

ε (m)	Preprocessing	Accuracy	Precision
0.5	None	0.43	0.45
0.5	SOR	0.49	0.51
0.5	ROR	0.33	0.36
1.0	None	0.54	0.53
1.0	SOR	0.57	0.59
1.0	ROR	0.37	0.44
2.0	None	0.51	0.53
2.0	SOR	0.55	0.62
2.0	ROR	0.38	0.41
3.0	None	0.39	0.42
3.0	SOR	0.41	0.38
3.0	ROR	0.22	0.28
4.0	None	0.42	0.43
4.0	SOR	0.43	0.37
4.0	ROR	0.16	0.19

Three observations are notable. First, SOR preprocessing consistently produced the highest accuracy and precision across all epsilon values, demonstrating that statistical neighbourhood-based outlier removal effectively improves the quality of input data for density-based clustering. The peak performance is achieved at ε = 1.0 m with SOR (accuracy: 0.57, precision: 0.59), closely followed by ε = 2.0 m with SOR (accuracy: 0.55, precision: 0.62 — the highest precision overall). At ε = 2.0 m, the precision exceeding accuracy suggests that whilst some true obstacle points are missed (lower accuracy), the points that are clustered are predominantly correct.

Journal of Information System and Technology Management
JISTM
EISSN: 0128-1666
Volume 11 Issue 44 (September 2026) PP. 236-257

Second, ROR preprocessing consistently degraded DBSCAN performance relative to both no-preprocessing and SOR conditions at every epsilon level. At ε = 4.0 m with ROR, accuracy falls to just 0.16 — worse than random classification for a balanced dataset. This degradation indicates that ROR over-removes sparse but valid maritime points (e.g., distant buoys or water-level coastline returns), eliminating the density features that DBSCAN relies upon for core-point identification.

Third, performance degrades at ε ≥ 3.0 m for all preprocessing conditions, confirming over-merging: at ε = 3.0 m, the average accuracy for None/SOR/ROR is 0.34 compared to 0.49 at ε = 1.0 m. In the harbour environment, an epsilon of 3 m is sufficiently large to incorporate points from adjacent obstacles (e.g., a moored vessel and its nearby buoy), collapsing distinct obstacle clusters into a single merged cluster and inflating FP counts.

ECE Clustering Performance

Table 6: ECE Clustering Results

MaxDistance (m)	Preprocessing	Accuracy	Precision
1.0	None	0.39	0.44
1.0	SOR	0.34	0.47
1.0	ROR	0.29	0.38
2.0	None	0.32	0.39
2.0	SOR	0.38	0.37
2.0	ROR	0.19	0.24
3.0	None	0.37	0.42
3.0	SOR	0.27	0.44
3.0	ROR	0.23	0.37

ECE demonstrated consistently lower accuracy than DBSCAN across all tested configurations, with the best result of accuracy 0.39 achieved at maxDistance = 1.0 m without preprocessing. Unlike DBSCAN, ECE accuracy does not benefit from SOR preprocessing at maxDistance = 1.0 m (0.34 with SOR vs 0.39 without), suggesting that noise removal may over-reduce point density below the threshold needed for ECE to form complete clusters from sparse maritime returns. The absence of precision-recall convergence in ECE results — where precision occasionally exceeds DBSCAN values (e.g., 0.47 at maxDistance = 1.0 m, SOR) despite lower accuracy — reflects ECE's tendency to form small, precise clusters that miss many true obstacle points, inflating FN counts and reducing accuracy.

The non-monotonic relationship between maxDistance and ECE performance (accuracy peaks at 1.0 m, then declines at 2.0 m, before partially recovering at 3.0 m for no-preprocessing) suggests that ECE cluster formation is highly sensitive to distance threshold in irregular maritime point distributions. ROR preprocessing again produces the worst results within each maxDistance group, consistent with the pattern observed in DBSCAN experiments.

Comparative Analysis and RViz Mapping Output

Direct comparison across all tested configurations confirms DBSCAN with SOR preprocessing as the superior pipeline for maritime point cloud obstacle detection. DBSCAN's advantage over ECE — average accuracy improvement of 0.18 at the respective optimal configurations —

Journal of Information System and Technology Management
JISTM
EISSN: 0128-1666
Volume 11 Issue 44 (September 2026) PP. 236-257

stems from its inherent noise point assignment mechanism, which explicitly excludes low-density artefacts rather than forcibly assigning them to nearest clusters. In the maritime context, this distinction is critical: wave spray, water surface reflections, and sensor noise generate pervasive low-density point artefacts that ECE incorporates into clusters, but DBSCAN correctly labels as noise.

Figure 10 presents the final RViz mapping output from the best-performing pipeline (DBSCAN + SOR, ε = 1.0 m), showing the detected cluster overlay on the raw maritime point cloud. Red points indicate clustered obstacle detections, while white points represent the raw unprocessed LiDAR data. The visualisation demonstrates that the pipeline successfully clusters the boat hull and a nearby buoy as distinct obstacle regions, providing the spatial information required for navigation guidance system integration.

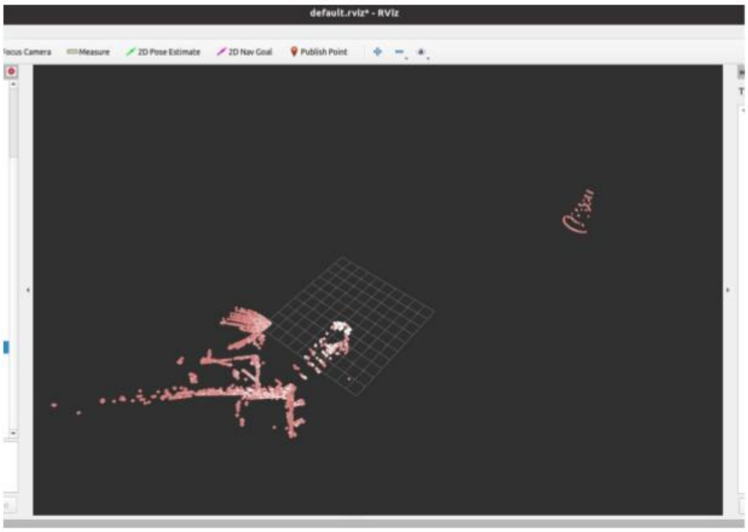

Figure 10: RViz Point Cloud Cluster Visualisation (DBSCAN + SOR, ε = 1.0 m): Red Points = Detected Obstacle Clusters; White Points = Raw Unprocessed LiDAR Data

The overall accuracy ceiling of approximately 57–60% across all configurations indicates a fundamental limitation of purely geometry-based clustering in maritime obstacle detection. In the Klang Harbour dataset, several confounding factors contribute to this ceiling: (1) wave-induced point cloud distortion that shifts obstacle boundary points into ambiguous spatial locations; (2) the absence of height-based ground plane removal applicable in terrestrial settings, as the water surface varies continuously; and (3) scale variability between obstacle types — bridge piers span metres while buoys occupy sub-metre volumes — which no single epsilon value can simultaneously optimise for. These limitations motivate the future development of multi-scale, classification-aware detection pipelines.

Discussion

The results consistently demonstrate that DBSCAN combined with SOR preprocessing constitutes the most effective pipeline for maritime point cloud obstacle detection among the configurations evaluated. The superiority of this combination can be attributed to the complementary roles of each method: SOR refines the point cloud by removing statistically anomalous points based on neighbourhood distribution, while DBSCAN's inherent noise-assignment mechanism further suppresses residual outliers during the clustering step itself.

Together, they address both the sparsity and stochastic noise characteristics intrinsic to maritime LiDAR data.

The inferior performance of ROR as a preprocessing step — despite its similar noise removal objective — can be attributed to its radius-only counting mechanism, which lacks the statistical range comparison that SOR employs. In maritime environments where genuine low-density regions exist alongside noise artefacts, ROR cannot reliably differentiate between the two, and risks discarding valid sparse features (such as distant buoys or coastline edges at the water line) whilst retaining false readings within dense wave-reflection clusters. The consistently worse performance of ROR-preprocessed inputs across all clustering configurations and epsilon values reinforces this interpretation. The optimal $N\_min \approx 5$ observed in ROR experiments corresponds approximately to the minimum reliable point density in the Klang Harbour dataset, below which returns cannot be distinguished from environmental noise.

The performance decline observed for DBSCAN at larger epsilon values ($\varepsilon \geq 3.0$ m) reflects the well-documented over-merging phenomenon: an overly permissive spatial radius causes geometrically proximate but semantically distinct obstacles to be incorrectly grouped into single clusters. This effect is especially pronounced in harbour environments where obstacles are irregularly spaced. The optimal epsilon range of 1.0–2.0 m balances cluster completeness with cluster separation in the Klang Harbour context, aligning with the typical inter-obstacle spacing observed in the annotated dataset.

ECE's consistent underperformance relative to DBSCAN can be explained by its absence of native noise handling. Without a mechanism to flag and exclude noise points, ECE is compelled to incorporate residual artefacts into clusters, inflating false positive counts and reducing both accuracy and precision. This finding underscores the importance of selecting clustering algorithms with inherent noise resistance for maritime applications characterised by sparse and distorted point cloud data. The partial recovery of ECE precision at maxDistance = 1.0 m suggests that tighter distance thresholds restrict ECE to genuine high-density obstacle cores, but at the cost of missing peripheral obstacle points and reducing accuracy.

The overall accuracy ceiling of approximately 60% highlights a fundamental limitation of geometry-based clustering approaches in maritime obstacle detection: the absence of object classification capability. Current methods detect spatially dense regions without discriminating between obstacle categories such as buoys, vessels, or coastline structures. This restricts the practical utility of the pipeline for USV guidance systems, which require classification-level situational awareness for safe and reliable autonomous navigation. Advanced frameworks employing mid-level LiDAR-stereo fusion, combined with deep learning-based object detectors such as YOLOv8 and hybrid PCA-K-Means clustering, have demonstrated substantially higher 3D Average Precision (82.6%) in comparable nearshore environments, underscoring the potential gains achievable through fusion-based architectures.

Conclusion

This study evaluated combinations of preprocessing and clustering algorithms for 3D LiDAR point cloud data in real maritime environments to support USV obstacle detection. Experimental results from Klang Harbour confirm that DBSCAN combined with SOR preprocessing achieves the highest performance among the tested configurations, peak accuracy of 0.57 ($\varepsilon = 1.0$ m) and peak precision of 0.62 ($\varepsilon = 2.0$ m). Voxel Grid Downsampling

Journal of Information System and Technology Management
JISTM
EISSN: 0128-1666
Volume 11 Issue 44 (September 2026) PP. 236-257
effectively reduces computational load proportionally with voxel size, and SOR consistently outperforms ROR as a maritime noise removal strategy across all tested clustering configurations. ECE clustering underperformed DBSCAN across all configurations, primarily due to the absence of inherent noise handling.

These findings provide empirical evidence for the superiority of density-based clustering with statistical preprocessing in maritime LiDAR processing contexts, contributing to the limited body of real-world validation studies for USV navigation systems. The results also demonstrate the inadequacy of ROR in maritime environments — specifically its failure to discriminate between genuine sparse features and noise artefacts — and establish epsilon = 1.0–2.0 m as the effective operating range for DBSCAN in harbour-scale scenarios. The optimal SOR parameters ($k = 1.0$, $r = 1.0$ m) and ROR minimum density threshold ($N\_min \approx 5$) are identified as practical baselines for future maritime point cloud processing pipelines.

However, the overall accuracy of approximately 60% remains below industrial operational requirements, and the absence of object classification capability represents a significant limitation for practical deployment. Future work should focus on three primary directions: (1) integration of point cloud model-based object detection — including PointPillars and VoxelNet architectures — to enable category-level classification of maritime obstacles beyond geometric grouping; (2) multi-sensor fusion combining LiDAR with stereo camera-based semantic segmentation, using mid-level feature fusion strategies to compensate for individual sensor deficiencies in low-visibility and wave-occluded conditions; and (3) investigation of real-time processing architectures, including RTOS-based and embedded GPU platforms such as the NVIDIA Jetson series, to support high-throughput sensor fusion pipelines for fully autonomous maritime navigation. The baseline preprocessing pipeline established in this study provides the foundation upon which such advanced perception frameworks can be built and validated.

Acknowledgements:	The authors would like to express their sincere gratitude to the IIUM Engineering Merit Scholarship (KOEIEMS) for Outstanding Students for providing the necessary resources and support throughout the course of this research. Special appreciation is extended to colleagues and peers who contributed valuable insights and constructive feedback, which greatly enhanced the quality of this paper.
Funding Statement:	This research received financial support from Ministry of Higher Education (MoHE) Malaysia under Grant Number MyLAB22-002-0002. The funding body had no role in the design of the study, data collection, analysis, interpretation of results, or the decision to publish this manuscript.
Conflict of Interest Statement:	The authors declare that there is no conflict of interest regarding the publication of this paper. All authors have contributed to this work and approved the final version of the manuscript for submission to the International Journal of Information System and Technology Management (JISTM).
Ethics Statement:	This study did not involve any human participants, animals, or sensitive data requiring ethical approval. The authors confirm that the research was conducted in accordance with accepted academic integrity and ethical publishing standards.
Author Contribution Statement:	All authors contributed significantly to the development of this manuscript. Zulkifli Zainal Abidin was responsible for conceptualization, methodology, and overall supervision of the study. Aiman Norazaruddin handled data collection, analysis, and interpretation of results and contributed to the literature review, drafting, and critical revision of the manuscript. All authors read and approved the final version of the manuscript prior to submission.

Journal of Information System and Technology Management
JISTM
EISSN: 0128-1666
Volume 11 Issue 44 (September 2026) PP. 236-257

References

Ahmed, A., Ahmad, I., Hussain, T., Qin, Z., & Bhatt, C. M. (2023). A comprehensive review of advances, applications, and challenges in autonomous surface vehicles. *Robotics*, 12(2), 46. https://doi.org/10.3390/robotics12020046

Balta, H., Velagic, J., Bosschaerts, W., De Cubber, G., & Siciliano, B. (2018). Fast statistical outlier removal based method for large 3D point clouds of outdoor environments. *IFAC-PapersOnLine*, 51(22), 348–353. https://doi.org/10.1016/j.ifacol.2018.11.566

Benjamin, M. R., Schmidt, H., Newman, P. M., & Leonard, J. J. (2010). Nested autonomy for unmanned marine vehicles with MOOS-IvP. *Journal of Field Robotics*, 27(6), 834–875. https://doi.org/10.1002/rob.20370

Bovcon, B., Muhoč, J., Pers, J., & Kristan, M. (2021). MODS: A USV-oriented obstacle detection benchmark. *IEEE Transactions on Intelligent Transportation Systems*, 22(3), 1513–1523. https://doi.org/10.1109/TITS.2019.2963537

Damodaran, B., Nair, B. B., & Akhilraj, N. (2023). Challenges of LiDAR and camera fusion for water surface detection in autonomous maritime navigation. *Ocean Engineering*, 284, 115263.

Feng, Q., Cheng, S., & Meng, Y. (2020). A survey on autonomous surface vehicles: Control, perception, navigation, and safety. *IEEE Access*, 8, 221208–221233.

Hacinecipoglu, A. (2022). Point cloud-based human pose estimation using voxel grid downsampling. *Applied Sciences*, 12(9), 4559. https://doi.org/10.3390/app12094559

Jin, Y., Duan, Z., & Li, Z. (2019). Distance and velocity measurement of coherent LiDAR based on chirp pulse compression. *Sensors*, 19(10), 2313. https://doi.org/10.3390/s19102313

Li, Q., Chen, L., Li, M., Shaw, S. L., & Nüchter, A. (2014). A sensor-fusion drivable-region and lane-detection system for autonomous vehicle navigation in challenging road scenarios. *IEEE Transactions on Vehicular Technology*, 63(2), 540–555. https://doi.org/10.1109/TVT.2013.2281366

Liu, Z., Zhang, Y., Yu, X., & Yuan, C. (2016). Unmanned surface vehicles: An overview of developments and challenges. *Annual Reviews in Control*, 41, 71–93. https://doi.org/10.1016/j.arcontrol.2016.04.018

Manley, J. E. (2008). Unmanned surface vehicles: 15 years of development. *Proceedings of OCEANS 2008*. https://doi.org/10.1109/OCEANS.2008.5152052

Rhinal, P., Dhoot, S., Gupta, R., & Shah, K. (2020). A systematic review of LiDAR sensors technology: Principles and challenges. *International Journal of Mechanical Engineering and Technology*, 11(6), 1–20.

Szutor, V., & Zichar, M. (2023). Comparative analysis of point cloud outlier removal methods. *Journal of Engineering and Applied Sciences*, 70(1), 1–14.

Talpur, A. H., Nawaz, M., Bhutto, A. H., & Lohano, S. (2025). Domain shift challenges in maritime perception: A survey. *Ocean Engineering*, 301, 117500.

Yu Cao, Z., Zhang, Y., & Li, R. (2021). Are we ready for unmanned surface vehicles in inland waterways? The USVInland multisensor dataset and benchmark. *IEEE Robotics and Automation Letters*, 6(2), 3964–3971. https://doi.org/10.1109/LRA.2021.3067271

Zhou, B., He, Y., Qian, K., Ma, X., & Li, X. (2021). S4-SLAM: A real-time 3D LiDAR SLAM system for ground/water surface multi-scene outdoor applications. *Autonomous Robots*, 45(1), 1–18. https://doi.org/10.1007/s10514-020-09948-3